Model studies of topological phase transitions in materials with two types of magnetic atoms

Zhuoran He and Gang Xu*

Wuhan National High Magnetic Field Center and School of Physics, Huazhong University of Science and Technology, Wuhan 430074, China

We study the topological phase transitions induced by Coulomb engineering in three triangular-lattice Hubbard models, AB_2, AC_3, and B_2C_3, each of which consists of two types of magnetic atoms with opposite magnetic moments. The energy bands are calculated using the Schwinger boson method. We find that a topological phase transition can be triggered by the second-order (three-site) virtual processes between the two types of magnetic atoms, the strengths of which are controlled by the on-site Coulomb interaction U. This class of topological phase transitions has rarely been studied and may be realized in a variety of real magnetic materials.

I. INTRODUCTION

Topological phase transitions [1–4] play a key role in condensed-matter physics. Especially, magnetic topological systems [5–7] often exhibit rich topological phases due to the complicated interplay between electron-electron interactions, magnetic moments, and spin-orbit coupling, which have been attracting intensive research interest for years [8–10]. A general model for the description of magnetic topological insulators is the spin-orbit coupled Hubbard model [11,12] with on-site Coulomb interaction U. Previous works on Coulomb engineering and correlation-driven effects in magnetic topological systems have studied various aspects of this topic, including the Hartree-Fock mean-field theory [6,13], dynamical screening effects [14], and phase transitions due to magnetic exchange coupling [15–17] using the Schwinger boson method. These works mostly focus on systems with one type of magnetic atom, while the topological phase transitions in systems with two types magnetic atoms are comparatively less studied.

In this paper, we study systems with two types of magnetic atoms [18–21] with opposite magnetic moments. In such systems, the two types of magnetic atoms separately form two sets of Chern bands, which then interact via a type of second-order virtual process of order $O(t_1 t_2/U)$. These processes involve the hopping from one type of magnetic atom i to atom j via the other type of magnetic atom k as an intermediate site. We call these $(1/U)$-controlled virtual processes the three-site terms, which can induce interesting topological phase transitions. We study their effect in a two-dimensional (2D) hexagonal Hubbard model with three types of lattice sites, A, B, and C, forming triangular, honeycomb, and kagome sublattices, respectively. By putting spin-up and spin-down electrons on two of the three types of lattice sites, we consider AB_2, AC_3, and B_2C_3 models and realize $(1/U)$-controlled topological phase transitions as characterized by changes in the Chern numbers of the spin-up and spin-down bands. Our

results demonstrate the interplay between band topology and correlation effects and present Coulomb engineering as a powerful tool to manipulate the topological phases of matter, with potential applications in various solid-state physical systems.

The rest of the paper is organized as follows. In Sec. II, we give the general formalism of our downfolding technique in the Schwinger boson representation and obtain the low-energy effective Hamiltonian containing the three-site terms. In Sec. III, we apply our formalism to the AB_2, AC_3, and B_2C_3 lattice structures to demonstrate the $(1/U)$-controlled topological phase transitions. Section IV contains a summary and conclusions, with a discussion of potential materials to realize the topological phase transitions found in our model studies.

II. FORMALISM

Suppose an insulating magnetic material is described by the spin-orbit coupled Hubbard model [11,12]

$$H = \sum_{ij\alpha\beta} t_{ij}^{\alpha\beta} c_{i\alpha}^{\dagger} c_{j\beta} + U \sum_{i} n_{i\uparrow} n_{i\downarrow}, \tag{1}$$

where i and j are the site indices and α and β label the spin. Here $t_{ij}^{\alpha\beta}$ contains the spin-orbit coupling (SOC) effect. We have from the first-principles Hamiltonian that

$$t_{ij}^{\alpha\beta} = \langle i\alpha | \frac{\vec{p}^2}{2m_e} + V(\vec{r}) + H_{SO} | j\beta \rangle, \tag{2}$$

$$H_{SO} = \frac{\hbar}{4m_e^2 c^2} [\nabla V(\vec{r}) \times \vec{p}] \cdot \vec{\sigma}, \tag{3}$$

where $V(\vec{r})$ is the periodic crystal potential. In the large-U limit, electrons try to avoid double occupancy, and thus, each site becomes spin polarized to form different long-range orders such as ferromagnetism, antiferromagnetism, ferrimagnetism, etc. [22,23]. Our Hubbard model in Eq. (1) preserves the time-reversal (TR) symmetry, whereas TR is broken by the magnetic order formed due to large U, which can give rise to topological phases with nonzero Chern numbers.

*gangxu@hust.edu.cn

To study the large-U limit more conveniently, we go to the Schwinger boson representation [24,25], where the electron operator can be represented as

$$c_{i\sigma}^{\dagger} = b_{i\sigma}^{\dagger} h_i + \sigma d_i^{\dagger} b_{i\bar{\sigma}}, \qquad (4)$$

where $\sigma = \uparrow (+1)$, $\downarrow (-1)$ is the spin index, h_i and d_i are the fermionic holon and doublon operators, $b_{i\sigma}$ and $b_{i\bar{\sigma}}$ are the Schwinger boson operators, and $\bar{\sigma} = -\sigma$ is the opposite spin of σ. By using the downfolding formula [26,27]

$$H_{\text{eff}} = PHP - \frac{1}{U} PH\bar{P}HP + O\left(\frac{1}{U^2}\right), \qquad (5)$$

where P is the projection operator into the Hilbert space with no doubly occupied sites (doublons) and $\bar{P} = 1 - P$, we keep all $O(1/U)$ terms and ignore $O(1/U^2)$ and higher-order terms to obtain the low-energy effective Hamiltonian of the chargeons

$$H_{\text{eff}} = \sum_{ij} \tilde{t}_{ij} h_i h_j^{\dagger} = \sum_{ij} \tilde{t}_{ij} f_i^{\dagger} f_j. \qquad (6)$$

A particle-hole transformation has been done from the holons $h_i \mapsto f_i^{\dagger}$ to the chargeons, with the effective hopping amplitudes $\tilde{t}_{ij}$ given by

$$\tilde{t}_{ij} = \sum_{\alpha\beta} b_{i\alpha}^{\dagger} \left(t_{ij}^{\alpha\beta} - \frac{1}{U} \sum_{k\gamma\delta} \gamma\delta \, t_{ik}^{\alpha\delta} t_{kj}^{\gamma\beta} b_{k\delta}^{\dagger} b_{k\bar{\gamma}} \right) b_{j\beta}. \qquad (7)$$

The derivation of Eqs. (6) and (7) is given in Appendix A. For magnetically ordered systems, the bosonic operators can be viewed as c numbers in the Bose-Einstein condensation approximation [28,29]. Previous works on topological phase transitions mostly focus on those transitions induced by changes in the electronic hopping amplitudes $t_{ij}^{\alpha\beta}$, which may give rise to gap closing, band inversion [30,31], etc. Here with Eq. (7), we can study two more types of topological phase transitions in terms of $\tilde{t}_{ij}$, i.e., (i) those induced by changing the magnetic structure and (ii) those induced by $1/U$, which controls the strengths of the three-site virtual processes. This paper focuses on the latter situation. We consider gap closing of the chargeon bands induced by the change of Hubbard U without changing the magnetic structure. In tuning U, we make sure U is still in the large-U regime, and therefore, the $O(1/U^2)$ terms ignored are still negligible compared with the three-site terms of order $O(1/U)$ considered in Eq. (7).

For simplicity, we consider a special case for 2D systems in which the bare hopping $t_{ij}^{\alpha\beta} = t_{ij}^{\alpha} \delta_{\alpha\beta}$ conserves spin and the magnetic structure is collinear ferrimagnetic in the z direction. From Eq. (3), the SOC does not flip spin if the crystal field $\nabla V(\vec{r})$ and all hopping bonds (direction of $\vec{p}$) are within the xy plane. Since the magnetic moments have zero x and y components and no double occupancy is allowed in the large-U limit, every site can be occupied by only the spin-up electrons or the spin-down electrons. In such a situation, Eq. (7) simplifies to

$$\tilde{t}_{ij} = \sum_{\sigma} z_{i\sigma}^* z_{j\sigma} \left(t_{ij}^{\sigma} - \frac{1}{U} \sum_k t_{ik}^{\sigma} t_{kj}^{\sigma} |z_{k\bar{\sigma}}|^2 \right), \qquad (8)$$

where the bosonic operators $b_{i\sigma} \mapsto z_{i\sigma}$ have been mapped to c numbers. Now we have a Hamiltonian with two sets of
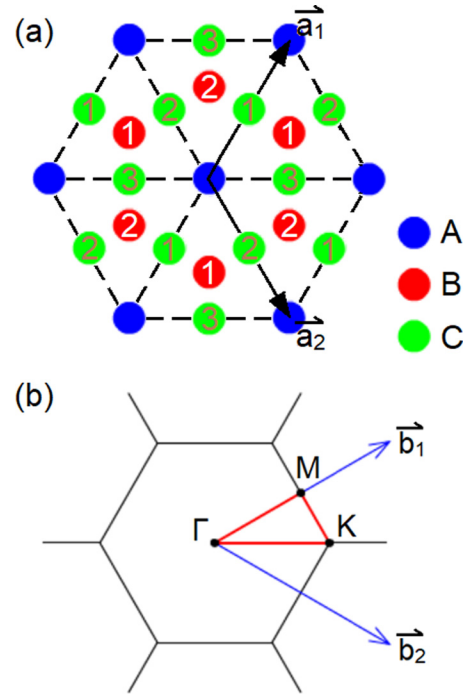

FIG. 1. (a) The 2D hexagonal lattice structure AB_2C_3. The A sites form a triangular lattice, the B sites form a honeycomb lattice, and the C sites form a kagome lattice, all sharing the same lattice vectors $\vec{a}_1$ and $\vec{a}_2$. (b) Brillouin zone with reciprocal lattice vectors $\vec{b}_1$ and $\vec{b}_2$ and high-symmetry path Γ-K-M-Γ.

bands formed by electrons on spin-up sites and spin-down sites, which interact via the second-order virtual processes described by the three-site $O(1/U)$ terms. In this paper, we use Eq. (8) as our simplified formula. Other magnetically ordered systems with more complex spin configurations such as noncollinear and spiral spin structures can be studied using Eq. (7).

III. RESULTS

To study the topological phase transitions within the framework of Eq. (8), we construct a 2D lattice structure AB_2C_3 with hexagonal symmetry [see Fig. 1(a)]. The A sites form a triangular lattice with one band, which is topologically trivial. The B sites form a honeycomb lattice with two bands, which realize the Haldane model [32]. The C sites form a kagome lattice with three bands. We will put opposite magnetic moments on two of the three types of lattice sites and consider electronic phases in the AB_2, AC_3, and B_2C_3 models, respectively. The three models can be considered special cases of the AB_2C_3 model where only two of the three types of lattice sites have magnetic moments and the magnetically neutral sites have been downfolded away.

A. The AB_2 structure

We consider an electronic phase with $N_{\uparrow} = N_{\downarrow} = 1$ per unit cell. In the case that the on-site orbital energy of an empty A site is lower than that of an empty B site, one of the spin species (e.g., the $\downarrow$ electrons) would first singly occupy the A sites. Then the other spin species (the $\uparrow$ electrons) would

not occupy the A sites because of the Hubbard U but instead occupy the B sites at an occupancy of 0.5. When the SOC is considered, the B sites become gapped, and the ↑ electrons realize the Haldane model [32] with real nearest-neighbor hopping t_1 and complex next-nearest-neighbor hopping t_2. We also consider a real *para*-position hopping t_3 among the B sites and denote the real nearest A-B site hopping as t. From Eq. (3), the SOC can make a hopping amplitude complex only when $\nabla V(\vec{r})$ is not parallel to $\vec{p}$, i.e., the bond direction. This implies that hopping amplitudes along bonds about which the crystal is symmetric should be real.

Following Eq. (8), the effective hopping amplitudes $\tilde{t}_{1-3}$ are given by

$$\tilde{t}_1 = \frac{1}{2}\left(t_1 - \frac{2t^2}{U}\right), \quad \tilde{t}_{2,3} = \frac{1}{2}\left(t_{2,3} - \frac{t^2}{U}\right). \quad (9)$$

Here we assume the boson fields $z_{A\downarrow} = 1$ and $z_{A\uparrow} = 0$ on the A sites and $z_{B\uparrow} = 1/\sqrt{2}$ and $z_{B\downarrow} = 0$ on the B sites. In Eq. (8), when the i and j labels are on the B sites, we have $\sigma = \uparrow$, and thus, the k label must be on the A sites, which are occupied by $\bar{\sigma} = \downarrow$, to mediate a three-site virtual process $j \to k \to i$. All three hoppings $\tilde{t}_{1-3}$ are renormalized by such three-site virtual processes. Due to the three-site-enhanced hopping $\tilde{t}_3$, the AB_2 model can now realize beyond-Haldane phases with occupied-band Chern numbers of ± 2.

In terms of the effective hoppings $\tilde{t}_{1-3}$, the spin-up Hamiltonian (i.e., a chargeon Hamiltonian restricted to the B sites) in the atomic gauge takes the form

$$H_B(\vec{k}) = \begin{bmatrix} 2\,\mathrm{Re}\,[\tilde{t}_2\zeta_2^*(\vec{k})] & \tilde{t}_1\zeta_1^*(\vec{k}) + \tilde{t}_3\zeta_1(2\vec{k}) \\ \tilde{t}_1\zeta_1(\vec{k}) + \tilde{t}_3\zeta_1^*(2\vec{k}) & 2\,\mathrm{Re}\,[\tilde{t}_2\zeta_2(\vec{k})] \end{bmatrix}, \quad (10)$$

where the functions $\zeta_{1,2}(\vec{k})$ are given by

$$\zeta_1(\vec{k}) = e^{i\vec{k}\cdot\frac{\vec{a}_1-\vec{a}_2}{3}} + e^{i\vec{k}\cdot\frac{\vec{a}_1+2\vec{a}_2}{3}} + e^{-i\vec{k}\cdot\frac{2\vec{a}_1+\vec{a}_2}{3}}, \quad (11a)$$

$$\zeta_2(\vec{k}) = e^{i\vec{k}\cdot\vec{a}_1} + e^{i\vec{k}\cdot\vec{a}_2} + e^{-i\vec{k}\cdot(\vec{a}_1+\vec{a}_2)}. \quad (11b)$$

We then use the integral of Berry curvature in the entire 2D Brillouin zone shown in Fig. 1(b) to calculate the Chern numbers [33]. A topological phase transition can be realized as shown in Fig. 2. In Fig. 2(a), the Hubbard $U = 10$ eV is large. The two spin species are clearly separated by the Hubbard interaction with almost forbidden three-site virtual hoppings. The spin-up electrons form a Haldane phase on the B sites with occupied-band Chern number $C_1 = +1$ and unoccupied-band Chern number $C_2 = -1$. The spin-down electrons fully occupy the triangular sites (A sites) and form a topologically trivial band (not plotted) with a Chern number of zero. As U gets smaller, the three-site virtual processes $\sim O(1/U)$ become stronger, and the *para*-position hopping $\tilde{t}_3$ is significantly enhanced. The band gap in Fig. 2(a) then closes at the M point at critical $U = 5.3$ eV and reopens as U is further reduced to form a beyond-Haldane phase with $C_1 = -2$ and $C_2 = +2$ [see Fig. 2(b) for $U = 4$ eV]. In fact, the transition can be driven by small changes in U across the critical value.

Since the contribution t^2/U of the second-order virtual processes is real, the imaginary part $\mathrm{Im}\,\tilde{t}_2 = \mathrm{Im}\,t_2$ remains unaffected by U. Therefore, the system can undergo topological phase transitions between $C_1 = +1 \leftrightarrow -2$ (if $\mathrm{Im}\,t_2 > 0$) and
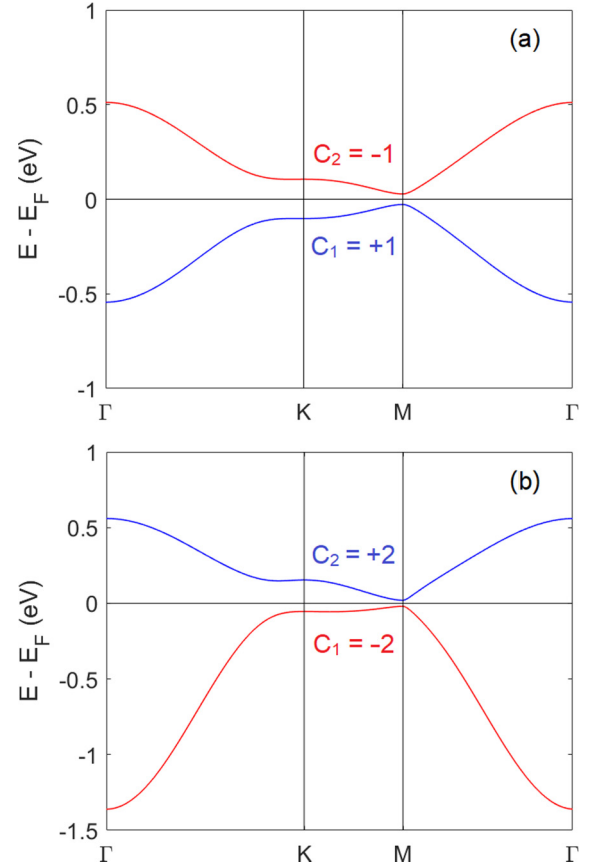

FIG. 2. The Chern bands of the B sites (honeycomb) in the AB_2 model. Hopping amplitudes $t_1 = -0.15$ eV, $t_2 = (0.06 + 0.04i)$ eV, $t_3 = -0.01$ eV, $t = 0.8$ eV. Hubbard $U = 10$ eV in (a), and $U = 4$ eV in (b). The Chern numbers $C_{1,2}$ indicate a topological phase transition (critical $U = 5.3$ eV).

$C_1 = -1 \leftrightarrow +2$ (if $\mathrm{Im}\,t_2 < 0$) but not in between the $C_1 = \pm 1$ (or ± 2) phases by tuning the Hubbard U.

B. The AC_3 structure

Consider an electronic phase in which the A sites are singly occupied by the ↓ electrons and the C sites are occupied by the ↑ electrons at occupancy $1/3$. The situation is similar to AB_2, except that the C sites form a kagome lattice. We consider the nearest-neighbor and next-nearest-neighbor hoppings t_1 and t_2 and real *para*-position hopping t_3 of the C-site hexagons. Both t_1 and t_2 can be complex. The real nearest-neighbor A-C site hopping is denoted as t. From Eq. (8), we have

$$\tilde{t}_{1-3} = \frac{1}{3}\left(t_{1-3} - \frac{t^2}{U}\right), \quad (12)$$

assuming $z_{A\downarrow} = 1$ and $z_{A\uparrow} = 0$ for the A sites and $z_{C\uparrow} = 1/\sqrt{3}$ and $z_{C\downarrow} = 0$ for the C sites. In terms of $\tilde{t}_{1-3}$, the C-site kagome Hamiltonian takes the form

$$H_C(\vec{k}) = \sum_{\nu=1}^{3} H_C^{(\nu)}(\vec{k}), \quad (13)$$
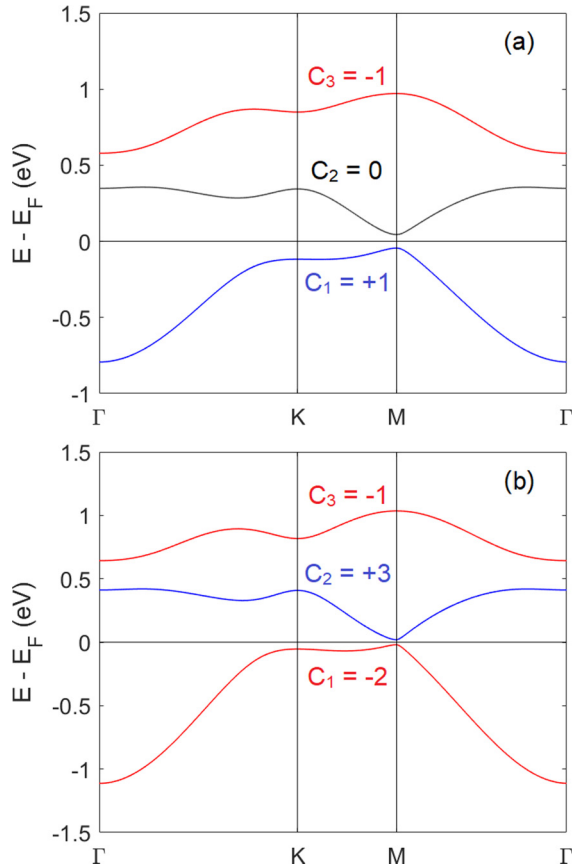
FIG. 3. The Chern bands of the C sites (kagome) in the AC_3 structure. Hopping amplitudes $t_1 = -(0.6 + 0.2i)$ eV, $t_2 = (0.1 + 0.1i)$ eV, $t_3 = -0.25$ eV, $t = 0.8$ eV. Hubbard $U = 10$ eV in (a), and $U = 4$ eV in (b). The Chern numbers C_{1-3} indicate a topological phase transition (critical $U = 4.9$ eV).

FIG. 4. The Chern bands of the C sites in the B_2C_3 model. Hopping amplitudes $t_1 = (0.6 - 0.1i)$ eV, $t_2 = -(0.1 + 0.02i)$ eV, $t = 0.8$ eV, $t' = (0.1 + 0.1i)$ eV. Hubbard $U = 10$ eV in (a), and $U = 4$ eV in (b). The Chern numbers C_{1-3} indicate a topological phase transition (critical $U = 5.3$ eV).

where the nearest-neighbor hopping $H_C^{(1)}(\vec{k})$, the next-nearest-neighbor hopping $H_C^{(2)}(\vec{k})$, and the *para*-position hopping $H_C^{(3)}(\vec{k})$ Hamiltonians are given specifically in Appendix B. A topological phase transition analogous to the AB_2 situation is realized in Fig. 3. In Fig. 3(a), the Hubbard $U = 10$ eV is large, and the three-site virtual hoppings are almost forbidden. As U gets smaller, the *para*-position hopping $\tilde{t}_3$ is significantly enhanced. The occupied-band Chern number changes from $C_1 = +1$ [see Fig. 3(a)] to $C_1 = -2$ [see Fig. 3(b)] when the gap closes at the M point at critical $U = 4.9$ eV. In the meantime, the Chern number C_2 of the middle band changes from 0 to $+3$, and the Chern number of the flat band on the top $C_3 = -1$ remains unchanged.

In Sec. III A and this section, we study the enhancement effect of the *para*-position hopping $\tilde{t}_3$ due the three-site virtual processes proportional to $1/U$. We find that in both the honeycomb and kagome lattices, the three-site processes can lead to topological phase transitions of $C_1 = +1 \leftrightarrow -2$ (or, symmetrically, $C_1 = -1 \leftrightarrow +2$) by closing the band gap at the M point. Because t^2/U is real, we cannot realize topological phase transitions between the $C_1 = \pm 1$ phases. We will demonstrate in Sec. III C that the $+1 \leftrightarrow -1$ transitions can be realized in the B_2C_3 model by making the contributions of the three-site processes $O(tt'/U)$ complex.
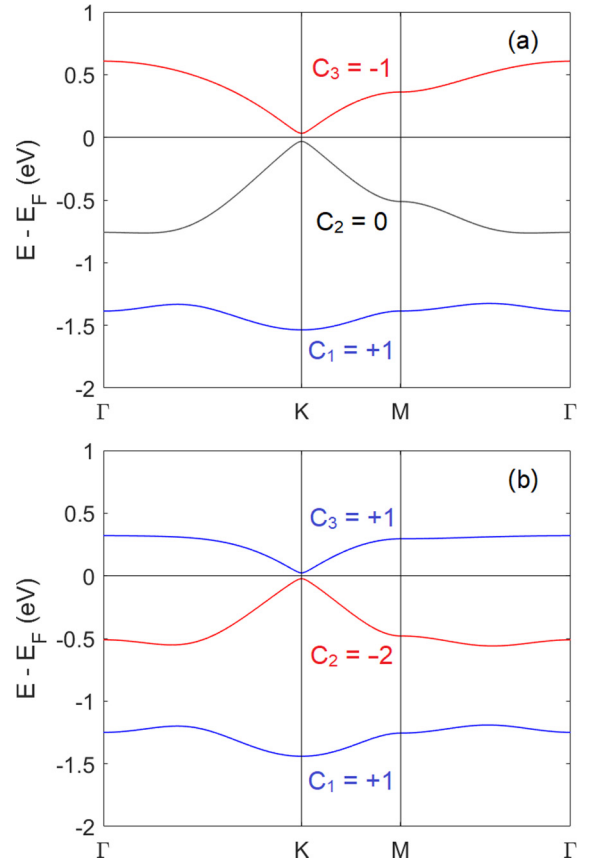
C. The B_2C_3 structure

In this section, we consider an electronic phase with $N_\uparrow = N_\downarrow = 2$ per unit cell. Let the two B sites in a unit cell be singly occupied by the $\downarrow$ electrons and the three C sites be occupied by $\uparrow$ electrons at an occupancy of 2/3. We consider the hoppings t and t' between the B-C sites and hoppings t_1 and t_2 among the C sites, as shown in Fig. 5. Since the total Chern number of the two spin-down bands on the B sites is zero [see Fig. 2(a)], we focus on the topological properties of the kagome bands, which are controlled by $1/U$. From Eq. (8), we have

$$\tilde{t}_1 = \frac{2}{3}\left(t_1 - \frac{t^2}{U}\right), \quad \tilde{t}_2 = \frac{2}{3}\left(t_2 - \frac{2tt'}{U}\right), \quad (14)$$

assuming $z_{B\downarrow} = 1$, $z_{B\uparrow} = 0$, $z_{C\uparrow} = \sqrt{2/3}$, and $z_{C\downarrow} = 0$. The *para*-position hopping $\tilde{t}_3 = 0$ of the kagome lattice is ignored. Even though $\tilde{t}_3$ can be mediated by t'^2/U, these contributions are small assuming $|t| \gg |t'|$. Notice that the B-C-site hopping t is real, while t' can be complex due to SOC. We define for $\uparrow$ electrons that the blue line hoppings in Fig. 5 are t' in clockwise directions and $(t')^*$ in counterclockwise directions. The Hamiltonian $H_C(\vec{k})$ is still given in Appendix B, with the effective hoppings $\tilde{t}_{1,2}$ now given by Eq. (14). A topological phase transition is realized, as shown in Fig. 4.
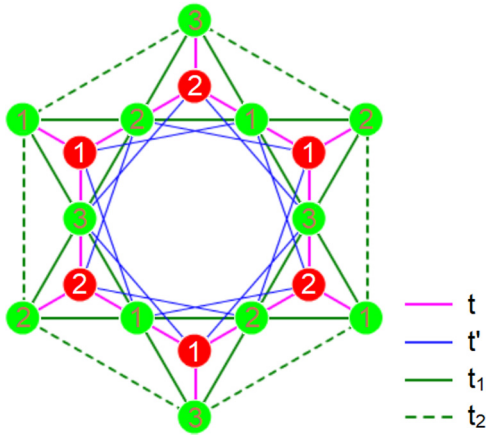
FIG. 5. The hoppings considered in B_2C_3. Here t and t' are between the B and C sites, and t_1 and t_2 are the nearest-neighbor and next-nearest-neighbor hoppings of the C-site kagome lattice. All hoppings except t can be complex due to the SOC. The *para*-position hoppings are ignored.

FIG. 6. Possible realizations of the AB_2C_3 lattice in a 3D hexagonal crystal structure with (a) alternating AB_2 and C_3 layers and (b) alternating AC_3 and B_2 layers. Both structures have the $P6/mmm$ space group symmetry.

In Fig. 4(a), the Hubbard $U = 10$ eV, and the occupied-band Chern number $C_1 + C_2 = +1$, which is determined by the imaginary parts Im $\tilde{t}_{1,2}$ of the effective hoppings in the kagome lattice. As U gets smaller, since t^2/U is real, Im $\tilde{t}_1$ remains unchanged, so only the tt'/U term in Eq. (14) can affect Im $\tilde{t}_2$. The band gap closes at the K point at critical $U = 5.3$ eV and then reopens to give rise to a $C_1 + C_2 = -1$ phase as U further decreases to 4 eV [see Fig. 4(b)]. The Chern number of the flat band at the bottom $C_1 = +1$ remains unchanged throughout the process. Because the imaginary part of the hopping amplitudes can be tuned by $1/U$, the phase separation between Chern numbers ± 1 is broken. A topological phase transition between the ± 1 phases can now be realized by tuning the Hubbard U due to the complex virtual hopping $O(tt'/U)$.

IV. CONCLUSION

We have demonstrated in this paper that the three-site virtual processes in the large-U limit of the Hubbard model can exhibit interesting renormalization effects of the hopping amplitudes and can give rise to topological phase transitions in the low-energy effective theory. We constructed 2D lattice models to realize the $1/U$ control of the honeycomb and kagome lattices. In the AB_2 model, a topological phase transition between the Haldane phase [32,34] and beyond-Haldane phase is realized by considering the enhancement effect of the *para*-position hopping $\tilde{t}_3$ due to the A-site mediated virtual hoppings proportional to $1/U$. The AC_3 model realizes a similar phase transition on the kagome lattice [35,36]. Both transitions close the band gap at the M point. In the B_2C_3 model, we also realized topological phase transitions on the kagome lattice, but the band gap closes at the K point. The contribution $O(tt'/U)$ of the three-site processes can be complex and drives the system across the phases boundary of occupied-band Chern number $= \pm 1$.

The phase transitions found in our model studies are realized using collinear antiferromagnetic (or ferrimagnetic) spin configurations. The spin-up and spin-down electrons occupy
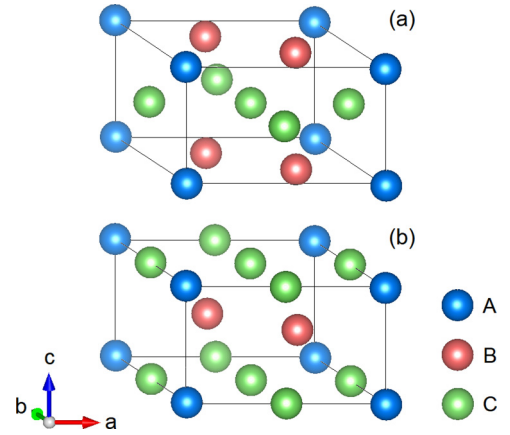
inequivalent lattice sites. In the examples shown in this paper, for simplicity, we let one spin species fully occupy one type of lattice site to be topologically trivial and use them to control the topological phase of the other spin species via the three-site terms. Interesting directions for further studies could be having both spin species exhibit topological properties and mutually influence each other via the three-site terms and the realization of similar Coulomb engineering effects in non-collinear spin systems. The Coulomb manipulation of surface states due to the topological phase transitions described in this paper could also be an important direction for future research.

Finally, we would like to discuss the possible realizations of our model in real materials. The $(1/U)$-controlled topological phase transitions can be realized without restricting the atoms to the same 2D plane. Two possible three-dimensional (3D) structures are shown in Fig. 6, both with $P6/mmm$ symmetry. Examples of materials with the structure in Fig. 6(a) are $R\mathrm{Co}_3\mathrm{B}_2$ [37], with R = rare-earth elements, $\mathrm{GdNi}_3\mathrm{Ga}_2$ [38], etc., which are potential candidates for the AC_3 model with two types of magnetic atoms. Coplanar AC_3 candidates include TiNi_3-type compounds [39–41] with shifted layers of close-packed AC_3 structures. Candidates for the AB_2 model include $\mathrm{UNi}_2\mathrm{Al}_3$ [42], $\mathrm{EuCo}_2\mathrm{Al}_9$ [43], etc. In particular, $\mathrm{EuCo}_2\mathrm{Al}_9$ has the entire AB_2C_3 structure [Fig. 1(a)] in one 2D plane, and all six of the other Al atoms are out of plane. We expect our work to be interesting to the fields of magnetism in alloys, ferrimagnets, and other materials with multiple types of magnetic atoms.

APPENDIX A: DERIVATION OF THE LOW-ENERGY EFFECTIVE HAMILTONIAN

By plugging Eq. (1) into Eq. (5), one obtains

$$H_{\text{eff}} = \sum_{ij\alpha\beta} t_{ij}^{\alpha\beta} P c_{i\alpha}^\dagger c_{j\beta} P - \frac{1}{U} \sum_{ijkl} \sum_{\alpha\beta\gamma\delta} t_{ij}^{\alpha\beta} t_{kl}^{\gamma\delta} P c_{i\alpha}^\dagger c_{j\beta} \bar{P} c_{k\gamma}^\dagger c_{l\delta} P. \tag{A1}$$

Then plugging in Eq. (4), one finds that the projections P pick out the following terms:

$$H_{\text{eff}} = \sum_{ij\alpha\beta} t_{ij}^{\alpha\beta} h_i h_j^\dagger b_{i\alpha}^\dagger b_{j\beta} - \frac{1}{U} \sum_{ijkl} \sum_{\alpha\beta\gamma\delta} \beta\gamma \, t_{ij}^{\alpha\beta} t_{kl}^{\gamma\delta} \, b_{i\alpha}^\dagger b_{j\bar{\beta}}^\dagger \, b_{k\bar{\gamma}} \, b_{l\delta} \, h_i \, (P d_j d_k^\dagger P) \, h_l^\dagger. \tag{A2}$$

The bosonic operators are automatically normal ordered. Notice that $P d_j d_k^\dagger P = \delta_{jk}$ because the doublon created must also be the doublon destructed to go back to the no-doublon subspace. One may then set $j = k$ and rename the dummy indices $l \mapsto j$ and $\beta \leftrightarrow \delta$ to obtain

$$H_{\text{eff}} = \sum_{ij} h_i h_j^\dagger \left[\sum_{\alpha\beta} b_{i\alpha}^\dagger \left(t_{ij}^{\alpha\beta} - \frac{1}{U} \sum_k \sum_{\gamma\delta} \gamma\delta \, t_{ik}^{\alpha\delta} t_{kj}^{\gamma\beta} \, b_{k\bar{\delta}}^\dagger \, b_{k\bar{\gamma}} \right) b_{j\beta} \right]. \tag{A3}$$

This result agrees with Eqs. (6) and (7) in the main text by defining the quantity in the square brackets as $\tilde{t}_{ij}$. All $O(1/U)$ renormalizations of $\tilde{t}_{ij}$ are considered in this formalism. Then we do a particle-hole transformation $h_i \mapsto f_i^\dagger$ to the holon operators and map the bosonic operators $b_{i\sigma} \mapsto z_{i\sigma}$ to c numbers and obtain

$$H_{\text{eff}} = \sum_{ij} f_i^\dagger f_j \left[\sum_{\alpha\beta} z_{i\alpha}^* z_{j\beta} \left(t_{ij}^{\alpha\beta} - \frac{1}{U} \sum_{k\gamma\delta} \gamma\delta \, t_{ik}^{\alpha\delta} t_{kj}^{\gamma\beta} \, z_{k\bar{\delta}}^* z_{k\bar{\gamma}} \right) \right] = \sum_{ij} \tilde{t}_{ij} f_i^\dagger f_j. \tag{A4}$$

In the special case in which the bare hopping $t_{ij}^{\alpha\beta} = t_{ij}^\alpha \delta_{\alpha\beta}$ conserves spin, we have

$$\tilde{t}_{ij} = \sum_{\alpha\beta} z_{i\alpha}^* z_{j\beta} \left(t_{ij}^\alpha \delta_{\alpha\beta} - \frac{1}{U} \sum_k \alpha\beta \, t_{ik}^\alpha t_{kj}^\beta z_{k\bar{\alpha}}^* z_{k\bar{\beta}} \right). \tag{A5}$$

Then the collinear ferrimagnetic structure in the z direction (perpendicular to the 2D lattice plane) with no double occupancy eliminates the $\alpha \neq \beta$ terms because site k can be occupied by only one type of spin species. Therefore, one obtains Eq. (8) in the main text.

APPENDIX B: KAGOME HAMILTONIAN IN TERMS OF $\tilde{t}_{1-3}$

In terms of the effective hoppings $\tilde{t}_{1-3}$, the full kagome Hamiltonian $H_C(\vec{k})$ contains three parts, as defined by Eq. (13): the nearest-neighbor hopping Hamiltonian is given by

$$H_C^{(1)}(\vec{k}) = \begin{bmatrix} 0 & 2\tilde{t}_1 \cos\left(\vec{k} \cdot \frac{\vec{a}_1 + \vec{a}_2}{2}\right) & 2\tilde{t}_1^* \cos\left(\vec{k} \cdot \frac{\vec{a}_2}{2}\right) \\ 2\tilde{t}_1^* \cos\left(\vec{k} \cdot \frac{\vec{a}_1 + \vec{a}_2}{2}\right) & 0 & 2\tilde{t}_1 \cos\left(\vec{k} \cdot \frac{\vec{a}_1}{2}\right) \\ 2\tilde{t}_1 \cos\left(\vec{k} \cdot \frac{\vec{a}_2}{2}\right) & 2\tilde{t}_1^* \cos\left(\vec{k} \cdot \frac{\vec{a}_1}{2}\right) & 0 \end{bmatrix}, \tag{B1}$$

the next-nearest-neighbor hopping Hamiltonian is given by

$$H_C^{(2)}(\vec{k}) = \begin{bmatrix} 0 & 2\tilde{t}_2 \cos\left(\vec{k} \cdot \frac{\vec{a}_1 - \vec{a}_2}{2}\right) & 2\tilde{t}_2^* \cos\left[\vec{k} \cdot \left(\vec{a}_1 + \frac{\vec{a}_2}{2}\right)\right] \\ 2\tilde{t}_2^* \cos\left(\vec{k} \cdot \frac{\vec{a}_1 - \vec{a}_2}{2}\right) & 0 & 2\tilde{t}_2 \cos\left[\vec{k} \cdot \left(\frac{\vec{a}_1}{2} + \vec{a}_2\right)\right] \\ 2\tilde{t}_2 \cos\left[\vec{k} \cdot \left(\vec{a}_1 + \frac{\vec{a}_2}{2}\right)\right] & 2\tilde{t}_2^* \cos\left[\vec{k} \cdot \left(\frac{\vec{a}_1}{2} + \vec{a}_2\right)\right] & 0 \end{bmatrix}, \tag{B2}$$

and the *para*-position hopping Hamiltonian is given by

$$H_C^{(3)}(\vec{k}) = \begin{bmatrix} 2\tilde{t}_3 \cos(\vec{k} \cdot \vec{a}_1) & 0 & 0 \\ 0 & 2\tilde{t}_3 \cos(\vec{k} \cdot \vec{a}_2) & 0 \\ 0 & 0 & 2\tilde{t}_3 \cos[\vec{k} \cdot (\vec{a}_1 + \vec{a}_2)] \end{bmatrix}, \tag{B3}$$

all written in the atomic gauge. In the AC_3 model, we consider the $1/U$ control of all three effective hoppings $\tilde{t}_{1-3}$. In the B_2C_3 model, we restrict ourselves to $\tilde{t}_{1-2}$, i.e., setting $\tilde{t}_3 = 0$.

[1] S. Sen, P. J. Wong, and A. K. Mitchell, The Mott transition as a topological phase transition, Phys. Rev. B **102**, 081110(R) (2020).

[2] S. Rufo, N. Lopes, M. A. Continentino, and M. A. R. Griffith, Multicritical behavior in topological phase transitions, Phys. Rev. B **100**, 195432 (2019).

[3] N. P. Mitchell, L. M. Nash, and W. T. M. Irvine, Realization of a topological phase transition in a gyroscopic lattice, Phys. Rev. B **97**, 100302(R) (2018).

[4] Y. Wang and L. Fu, Topological Phase Transitions in Multicomponent Superconductors, Phys. Rev. Lett. **119**, 187003 (2017).

[5] D. Nevola, H. X. Li, J.-Q. Yan, R. G. Moore, H.-N. Lee, H. Miao, and P. D. Johnson, Coexistence of Surface Ferromagnetism and a Gapless Topological State in $MnBi_2Te_4$, Phys. Rev. Lett. **125**, 117205 (2020).

[6] V. Ivanov, X. Wan, and S. Y. Savrasov, Topological Insulator-to-Weyl Semimetal Transition in Strongly Correlated Actinide System UNiSn, Phys. Rev. X **9**, 041055 (2019).

[7] J. Wang, B. Lian, and S.-C. Zhang, Electrically Tunable Magnetism in Magnetic Topological Insulators, Phys. Rev. Lett. **115**, 036805 (2015).

[8] X. Zhai and G. Jin, Photoinduced topological phase transition in epitaxial graphene, Phys. Rev. B **89**, 235416 (2014).

[9] L. Wang, H.-H. Hung, and M. Troyer, Topological phase transition in the Hofstadter-Hubbard model, Phys. Rev. B **90**, 205111 (2014).

[10] Z. Cai, S. Chen, S. Kou, and Y. Wang, Properties of a class of topological phase transitions, Phys. Rev. B **78**, 035123 (2008).

[11] C. De Franco, L. F. Tocchio, and F. Becca, Metal-insulator transitions, superconductivity, and magnetism in the two-band Hubbard model, Phys. Rev. B **98**, 075117 (2018).

[12] K. Misumi, T. Kaneko, and Y. Ohta, Mott transition and magnetism of the triangular-lattice Hubbard model with next-nearest-neighbor hopping, Phys. Rev. B **95**, 075124 (2017).

[13] Q. Zhu, Q. Tong, H. Sun, Y. Wang, and W. Yao, Coulomb effects on topological band inversion in the moiré of WSe_2/BAs heterobilayer, 2D Mater. **6**, 045037 (2019).

[14] M. Rösner and J. L. Lado, Coulomb-engineered topology, Phys. Rev. Research **3**, 013265 (2021).

[15] X. Lei and Z. Jun, Slave-fermion mean-field theory of Heisenberg model, Commun. Theor. Phys. **48**, 363 (2007).

[16] D. Yoshioka, Slave-fermion mean field theory of the Hubbard model, J. Phys. Soc. Jpn. **58**, 1516 (1989).

[17] C. Jayaprakash, H. R. Krishnamurthy, and S. Sarker, Mean-field theory for the $t - J$ model, Phys. Rev. B **40**, 2610 (1989).

[18] H. Ohnishi, K. Katoh, and K. Motizuki, Magnetic phase diagram of system with two different atoms in unit cell, J. Magn. Magn. Mater. **31–34**, 55 (1983).

[19] M. Marcos, P. Romero, and J.-L. Serrano, Cheminform abstract: Nematic liquid crystal materials containing nickel(ii) or copper(ii) atoms. Two different kinds of magnetic behaviour, ChemInform **21** (1990).

[20] P. S. Wang, W. Ren, L. Bellaiche, and H. J. Xiang, Predicting a Ferrimagnetic Phase of Zn_2FeOsO_6 with Strong Magnetoelectric Coupling, Phys. Rev. Lett. **114**, 147204 (2015).

[21] M. Halder, S. M. Yusuf, M. D. Mukadam, and K. Shashikala, Magnetocaloric effect and critical behavior near the paramagnetic to ferrimagnetic phase transition temperature in $TbCo_{2-x}Fe_x$, Phys. Rev. B **81**, 174402 (2010).

[22] J. Gouveia and R. Dias, Magnetic phase diagram of the Hubbard model in the Lieb lattice, J. Magn. Magn. Mater. **382**, 312 (2015).

[23] G. Z. Wel, H. Q. Nie, and K. Y. Zhang, Correlation effects of the antiferromagnetic phase in the Hubbard model, Phys. Status Solidi B **156**, 363 (1989).

[24] F. Wang and R. Tao, Schwinger-boson approach to the two-dimensional antiferromagnetic Heisenberg model beyond the mean-field approximation, Phys. Rev. B **61**, 3508 (2000).

[25] J. Rech, P. Coleman, G. Zarand, and O. Parcollet, Schwinger Boson Approach to the Fully Screened Kondo Model, Phys. Rev. Lett. **96**, 016601 (2006).

[26] F. Ma, W. Purwanto, S. Zhang, and H. Krakauer, Quantum Monte Carlo Calculations in Solids with Downfolded Hamiltonians, Phys. Rev. Lett. **114**, 226401 (2015).

[27] G. Giovannetti, M. Casula, P. Werner, F. Mauri, and M. Capone, Downfolding electron-phonon Hamiltonians from *ab initio* calculations: Application to K_3 picene, Phys. Rev. B **90**, 115435 (2014).

[28] H. T. Ueda and K. Totsuka, Ground-state phase diagram and magnetic properties of a tetramerized spin-$1/2J_1$-J_2 model: BEC of bound magnons and absence of the transverse magnetization, Phys. Rev. B **76**, 214428 (2007).

[29] M. J. Davis, T. M. Wright, T. Gasenzer, S. A. Gardiner, and N. P. Proukakis, Formation of Bose-Einstein condensates, arXiv:1601.06197.

[30] B. M. Wojek, P. Dziawa, B. J. Kowalski, A. Szczerbakow, A. M. Black-Schaffer, M. H. Berntsen, T. Balasubramanian, T. Story, and O. Tjernberg, Band inversion and the topological phase transition in (Pb,Sn)Se, Phys. Rev. B **90**, 161202(R) (2014).

[31] D. Wang, L. Chen, H. Liu, C. Shi, X. Wang, G. Cui, P. Zhang, and Y. Chen, Strain induced band inversion and topological phase transition in methyl-decorated stanene film, Sci. Rep. **7**, 17089 (2017).

[32] F. D. M. Haldane, Model for a Quantum Hall Effect without Landau Levels: Condensed-Matter Realization of the "Parity Anomaly," Phys. Rev. Lett. **61**, 2015 (1988).

[33] X.-L. Qi and S.-C. Zhang, Topological insulators and superconductors, Rev. Mod. Phys. **83**, 1057 (2011).

[34] T. Thonhauser and D. Vanderbilt, Insulator/Chern-insulator transition in the Haldane model, Phys. Rev. B **74**, 235111 (2006).

[35] Y. Chen, S. Xu, Y. Xie, C. Zhong, C. Wu, and S. B. Zhang, Ferromagnetism and Wigner crystallization in kagome graphene and related structures, Phys. Rev. B **98**, 035135 (2018).

[36] H.-M. Guo and M. Franz, Topological insulator on the kagome lattice, Phys. Rev. B **80**, 113102 (2009).

[37] H. Ido, O. Nashima, T. Ito, T. Kaneda, Y. Saito, K. Konno, H. Yoshida, and M. Motokawa, Magnetic properties of RCo_3B_2 (R=rare-earth) compounds, J. Appl. Phys. **85**, 4865 (1999).

[38] S. Pechev, J.-L. Bobet, B. Chevalier, B. Darriet, and F. Weill, Relationship between the synthesis conditions and the structural, electrical, magnetic, and hydrogen absorption properties of the ternary compounds $GdNi_3X_2$ with X = Al, Ga, or Sn, J. Solid State Chem. **150**, 62 (2000).

[39] J.-H. Xu, W. Lin, and A. J. Freeman, Electronic structure and phase stability of A_3Ti (A=Fe, Co, Ni, and Cu), Phys. Rev. B **48**, 4276 (1993).

[40] B. Wodniecka, P. Wodniecki, M. Marszalek, and A. Hrynkiewicz, Electric quadrupole interaction at ^{181}Ta probes in hexagonal TiNi$_3$-type compounds, J. Alloys Compd. **219**, 128 (1995).

[41] M. D. Le, K. A. McEwen, E. Colineau, J.-C. Griveau, and R. Eloirdi, Magnetic and electrical properties of (Pu,Lu)Pd$_3$, Phys. Rev. B **82**, 155136 (2010).

[42] C. Geibel, A. Böhn, R. Caspary, K. Gloos, A. Grauel, P. Hellmann, R. Modler, C. Schank, G. Weber, and F. Steglich, Ground state properties of UNi$_2$Al$_3$ and UPd$_2$Al$_3$, Phys. B (Amsterdam, Neth.) **186–188**, 188 (1993).

[43] V. M. T. Thiede and W. Jeitschko, Crystal structure of europium cobalt aluminide (1/2/9), EuCo$_2$Al$_9$, Z. Kristallogr. - New Cryst. Struct. **214**, 149 (1999).